Journal of Design Intelligence
https://www.ffspub.com/index.php/jdi
ISSN 3104-9001 (print)
ISSN 3136-3032 (online)
E-mail: jdi.office@ffspub.com



Article

Dual-Metal Electron Pump Engineered Platinum-based HOR Catalysts for Ammonia-tolerant Hydrogen Sensing

Changqing Jin[1,2], Rui Wang[1,3,4,5,†], Aojie Zhang[1,3], Yanshen Zhao[1], Zemin Huang[5], Haolin Tang[1,3,4,†]
[1]*State Key Laboratory of Advanced Technology for Materials Synthesis and Processing, Wuhan University of Technology, Wuhan 430070, China*
[2]*State Key Laboratory of Molecular Engineering of Polymers, Department of Macromolecular Science, Fudan University, Shanghai, 200438, China*
[3]*National Energy Key Laboratory for new hydrogen-ammonia energy technologies, Foshan Xianhu Laboratory, Foshan 528200, China*
[4]*Hubei Key Laboratory of Fuel Cells, Wuhan University of Technology, Wuhan, 430070, China*
[5]*School of Chemistry and Chemical Engineering, Wuhan University of Technology, Wuhan 430070, China*
[†]*E-mail: rwang@whut.edu.cn (R.W.); thln@whut.edu.cn (H.T.)*

Received: October 22, 2026/ Revised: October 29, 2026/ Accepted: November 03, 2026/ Published online: November 05, 2026

Abstract: Electrochemical hydrogen sensors are attractive for hydrogen detection owing to their high sensitivity, rapid response, and low energy consumption, offering great potential for safety monitoring in complex environments. However, the anodic HOR catalysts are highly susceptible to poisoning by interfering species such as ammonia, posing a critical challenge to the development of robust hydrogen sensors for ammonia-containing environments. Since binary transition metal elements are promising for further optimizing the HOR performance of platinum compared to single transition metals, metal salts with different combinations were dispersed on XC-72 by rotary evaporation here. After wet impregnation, FeCo-Pt, FeMn-Pt, CoMn-Pt, and Fe-Pt, were obtained by heat treatment under H_2/Ar mixed gas. In this strategy, Fe and Co form an FeCo alloy during heat treatment. Compared to single-element doping, the alloyed transition metal acted as "dual-metal electron pump" further optimizes the electronic structure of Pt, thereby constructing a highly efficient composite catalyst system. This effective regulation of the electronic structure significantly enhances the electron transfer capability of Pt, ultimately achieving simultaneous improvements in the catalyst's HOR activity and ammonia resistance, thereby enabling efficient hydrogen sensing with strong resistance to disturbance.

Keywords: HOR; Hydrogen Sensing; Electrocatalyst; Dual-Metal; Electron Pump
https://doi.org/10.64509/jdi.14.173

1 Introduction

As the concept of low-carbon living gains popularity, hydrogen plays an irreplaceable role in the energy transition and storage area [1–3]. However, the safe storage, transportation, and end-use of hydrogen create an urgent need for real-time, precise concentration monitoring [4, 5]. Electrochemical hydrogen sensing technology, characterized by high sensitivity, rapid response, and low energy consumption, offers a promising technical pathway for hydrogen safety monitoring in complex environments [6–8]. The core operating principle of these sensors relies on the electrocatalytic hydrogen oxidation reaction (HOR); hydrogen concentration is determined by measuring changes in the HOR current signal [9]. Therefore, developing more efficient HOR catalysts for hydrogen sensing is a highly significant endeavor worthy of sustained investment, as it can substantially enhance safety in hydrogen-related applications by improving hydrogen detection resolution and response speed.

However, electrochemical hydrogen sensors face a significant challenge in practical applications: HOR catalysts are highly susceptible to poisoning by impurity gases [10, 11], with ammonia (NH_3) being a particularly critical interfering species. The strong adsorption of ammonia molecules onto the platinum (Pt) surface occupies catalytically active sites and blocks hydrogen adsorption and dissociation, leading to severe signal attenuation or even complete sensor failure [12].

† Corresponding author: Rui Wang, Haolin Tang
*Academic Editor: Yan Hong
© 2026 The authors. This article is an open access article distributed under the terms and conditions of the Creative Commons Attribution (CC BY) license (https://creativecommons.org/licenses/by/4.0/).

This issue is especially pronounced in technologies utilizing ammonia as a hydrogen storage medium [13, 14], where trace amounts of residual ammonia (remaining after hydrogen production via ammonia decomposition) directly poison the sensor electrodes, severely limiting the long-term stable operation of hydrogen sensors in ammonia-containing environments.

Ammonia poisoning of Pt-based catalysts typically manifests as rapid performance degradation and a significant decline in stability. When operating in ammonia-containing atmospheres, Pt-based catalysts are prone to deactivation due to the strong adsorption of nitrogenous species, resulting in a continuous decrease in output current and an increase in overpotential for fuel cells or sensors [15]. Current strategies to address this issue include charge modulation of the support and electronic modification via alloying. Wang *et al*. [16] systematically investigated the anti-poisoning mechanisms of PtM (M = Fe, Co, Ni, Cu, Zn) compounds using density functional theory (DFT); they found that the incorporation of Fe, Co, Cu, and Zn altered the electronic structure of Pt atoms, weakening the adsorption energy of ammonia on the surface of PtM compounds thereby enhancing resistance to poisoning. In the case of Fe/Y co-modulated Pt-based catalysts, Fe promoted the formation of a PtY alloy (rather than a stable Y-oxide phase), significantly reducing NH_3 adsorption energy and allowing the catalyst to retain 93.1% of its initial activity even in the presence of 5000 ppm NH_3. Jin *et al*. [10] prepared a Pt-N_2/KB catalyst (with a Pt loading of only 2.03 wt%) by modulating the charge distribution of Pt using a nitrogen-doped carbon support; this catalyst achieved a mass activity of 5.4 and 4.7 times higher than those of commercial 20% Pt/C, while also exhibiting a lower current decay rate in an electrochemical hydrogen purification device. DFT calculations revealed that the catalyst surface possessed a hydrogen adsorption free energy close to zero alongside lower ammonia adsorption energy, enabling a simultaneous enhancement of hydrogen oxidation reaction activity and resistance to ammonia poisoning. Wang *et al*.[17] elucidated the ammonia-tolerance mechanism of Cr-doped $MoNi_4$ from the perspective of nickel-based catalysts. Cr modification not only creates an electron-rich state that suppresses the lone-pair electron donor behavior of NH_3 but also shifts the d-band center downward to weaken d-electron back-donation, thereby synergistically reducing NH_3 adsorption. The catalyst exhibited no significant activity decay over 10,000 cycles in the presence of 2 ppm NH_3, and a fuel cell incorporating it retained 95% of its initial peak power density when 10 ppm NH_3/H_2 was fed, whereas a Pt/C-based cell retained only 61%. These examples demonstrate that, whether through charge modulation of the support or electronic modification via alloying, the core mechanism lies in tuning the electronic structure of Pt or the active sites to weaken the bonding strength with nitrogen-containing poisoning species while maintaining moderate H* adsorption, thereby achieving a synergistic optimization of ammonia tolerance and HOR activity.

This study systematically reveals how dual-metal electron pump which constructed by neighboring binary transition-metal alloys (FeCo-Pt is preferred) modulate the electronic structure of Pt and simultaneously enhance both HOR activity and resistance to ammonia poisoning. Compared to conventional single-element doping strategies, bimetallic alloying achieves finer and more effective control over Pt's electronic structure through the synergistic effects between the two transition metals. This strategy offers a design approach for developing robust electrochemical hydrogen sensors suitable for ammonia-containing environments. In technological pathways utilizing ammonia as a hydrogen storage medium, hydrogen sensors must operate stably over long periods in ammonia-rich atmospheres; thus, the catalyst's resistance to ammonia poisoning is a critical factor determining the sensor's service life and reliability. The bimetallic electronic pump modulation strategy proposed in this study is applicable not only to hydrogen sensors but also to other Pt-based electrocatalytic systems operating in ammonia-containing environments, such as anodes for proton exchange membrane fuel cells.

2 Physical Structure Characterization

The preparation process of the FeCo-Pt series catalysts is shown in Figure 1(a). 0.5167 g of $Fe(NO_3)_3{\cdot}6H_2O$ and 0.3528 g of $Co(NO_3)_2{\cdot}6H_2O$ were dissolved in 50 mL of deionized water and stirred under heating for 10 min. Then, 0.1 g of PVP was added, and the mixture was stirred in a water bath for 30 min until completely dissolved. After, 0.1 g of XC-72 was added, and stirring was continued for 2 h to ensure uniform dispersion. The mixture was rotary-evaporated at 65 °C for 150 min to remove water, then transferred to a vacuum drying oven and dried for 8 h to eliminate residual moisture. After grinding the product, 1 g of the powder was heat-treated at 950 °C for 30 min under a flow of 5% H_2/Ar mixed gas (50 mL/min); following thorough re-grinding, the sample was designated as FeCo-Pt. Three additional samples were prepared by keeping other steps constant but varying the precursors: by adding 0.2527 g of $Mn(NO_3)_2{\cdot}4H_2O$ alongside $Fe(NO_3)_3{\cdot}6H_2O$; by adding 0.2527 g of $Mn(NO_3)_2{\cdot}4H_2O$ alongside $Co(NO_3)_2{\cdot}6H_2O$; and using only $Fe(NO_3)_3{\cdot}6H_2O$. The deposition of Pt was conducted by wet impregnation as follow [18, 19]. The FeCo support (50 mg) was accurately weighed and dispersed in 20.45 mL of an aqueous $Pt(NO_3)_2$ solution. After vigorous stirring for 8 h, the mixture was subjected to rotary evaporation at 65 °C. After the water had been completely removed, the material was transferred to a vacuum drying oven for 8 h. The dried powder was transferred to a tube furnace, then slowly heated to 150 °C and held for 120 min under a flow of 5% H_2/Ar mixed gas (150 mL/min) to obtain the FeCo-Pt sample. FeMn-Pt, CoMn-Pt, and Fe-Pt were prepared using the same procedure.

The microstructures of the four electrocatalysts were characterized in detail using TEM to reveal their structural features and the dispersion of nanoparticles. As shown in Figure 1(b),(d), a large number of dark spots were observed in both the FeCo-Pt and Fe-Pt samples, indicating the uniform dispersion of Pt nanoparticles within the electrocatalysts. Additionally, large shaded regions were identified in both sets of samples, suggesting the presence of crystalline phases with

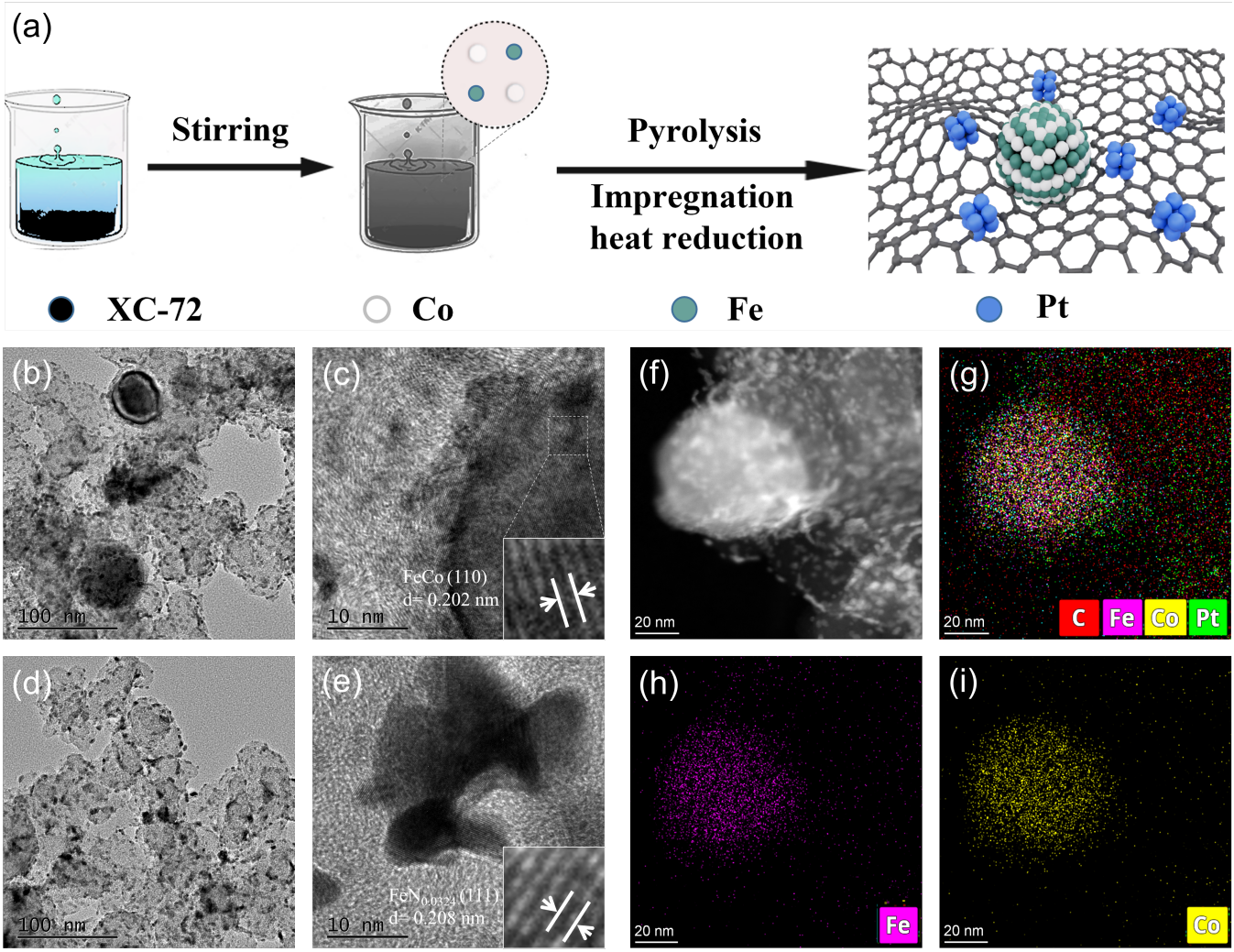


Figure 1: (a) Schematic diagram of the synthesis process for FeCo-Pt. TEM images for FeCo-Pt (b, c) and Fe-Pt (d, e). HAADF-STEM (f) and (g-i) EDS mapping of the individual elements of the Fe-Pt catalyst.

specific lattice structures; these regions were further characterized using HRTEM. The HRTEM results revealed that the crystals corresponding to the large shaded regions in the Fe-Pt sample exhibited a lattice spacing of 0.208 nm, matching the (111) crystal plane of $FeN_{0.0324}$ (as shown in Figure 1(e)). In contrast, the crystals corresponding to the shaded regions in the FeCo-Pt sample (Figure 1(c)) showed a lattice spacing of 0.202 nm, corresponding to the (110) crystal plane of the FeCo alloy [20]; notably, no $FeN_{0.0324}$ crystals were detected in the FeCo-Pt sample. This difference indicates that the introduction of Co promotes the formation of an FeCo alloy within the FeCo-Pt system. To further investigate the compositional and structural characteristics of the FeCo-Pt electrocatalyst, HAADF-STEM and EDS images were conducted in Figure 1(f–i). As shown in Figure 1(g), Pt is uniformly distributed throughout the FeCo-Pt catalyst; this uniform distribution helps increase the number of active sites, thereby enhancing electrochemical performance [21]. Meanwhile, the distribution of Fe highly overlaps with that of Co, concentrating in the regions of the FeCo alloy crystals surrounding fine platinum particles indicating that Fe and Co successfully alloyed during synthesis to form a stable FeCo alloy phase.

To further investigate the crystal structures of the four electrocatalyst supports, X-ray diffraction (XRD) was employed for characterization. As shown in Figure 2(a), the XRD pattern of the FeCo support sample exhibits three distinct, strong diffraction peaks at 44.88°, 65.31°, and 88.74°, corresponding to the (111), (200), and (211) crystal planes of the FeCo alloy; this aligns with TEM observations and further confirms the formation of the FeCo alloy within the sample. As shown in Figure 2(b), the diffraction peaks in the XRD pattern of the FeMn support correspond to the standard peaks for $Fe_{0.497}Mn_{0.503}O$ and $FeN_{0.0324}$, indicating the formation of these phases in the sample. As shown in Figure 2(c), the diffraction peaks in the XRD pattern of the CoMn support correspond to the standard peaks for MnO and Co, indicating the formation of MnO and Co [22]. These results demonstrate that when Mn coexists with Co, or Fe with Co, and the system undergoes heat treatment, the formation of oxide phases is favored over alloy structures. As shown in Figure 2(d), the diffraction peaks in the XRD pattern of the Fe support correspond to the standard peaks for $FeN_{0.0324}$, indicating the formation of iron nitrides. A comparison reveals that the introduction of Co significantly modulates phase formation within the system, shifting the Fe-based product

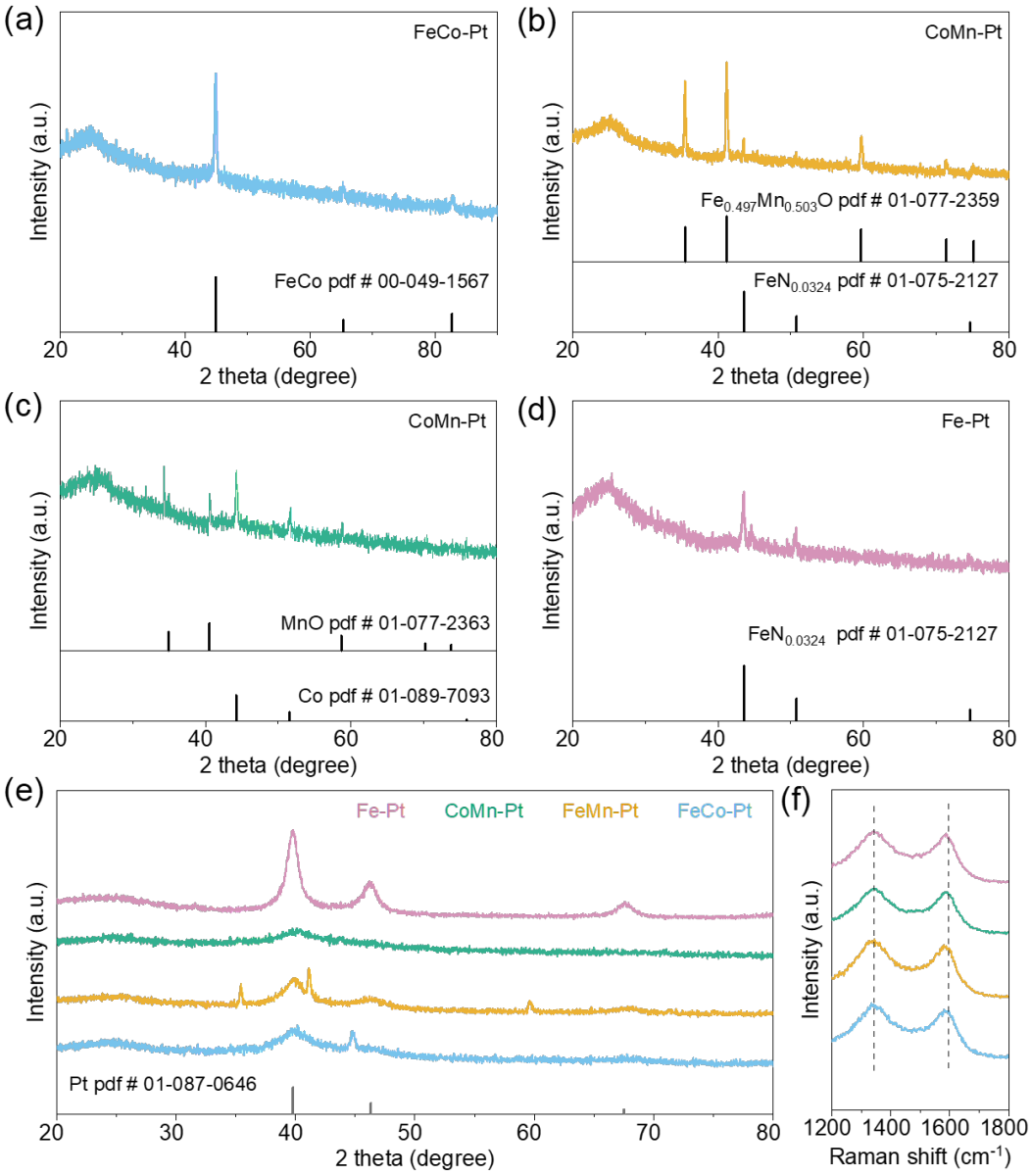


Figure 2: XRD patterns of (a) FeCo (b) FeMn (c) CoMn (d) Fe. XRD patterns (e) and Raman spectra (f) of the synthesized Pt catalysts.

from $FeN_{0.0324}$ to the FeCo alloy. Furthermore, while the co-pyrolysis of Fe and Mn yields $Fe_{0.497}Mn_{0.503}O$ crystals, the co-pyrolysis of Fe and Co results in the formation of MnO. These results indicate that the synergistic regulation by different transition metal elements significantly influences the crystal structure and electronic properties of the catalyst support, providing a theoretical basis for the further optimization of catalyst design and performance enhancement.

To further analyze the crystalline phase distribution of Pt in the four electrocatalysts following wet impregnation, standard Pt diffraction patterns were used as a reference to identify the Pt crystalline phases present on the supports. As shown in Figure 2(e), FeCo-Pt, FeMn-Pt, CoMn-Pt, and Fe-Pt all exhibited three new diffraction peaks at 39.8°, 46.3°, and 67.5°, corresponding to the (111), (200), and (220) crystal planes of Pt [23], respectively; this confirms the successful formation of Pt on the supports and aligns with the TEM observations. To further investigate the carbon structural characteristics, Raman spectroscopy was also employed. The D-band at around 1349.2 cm^{-1} is associated with defects and disorder in the carbon support, while the G-band at around 1588 cm^{-1} arises from the vibration of sp^2-hybridized carbon; the degree of defects in the carbon support was evaluated based on the intensity ratio of the D-band to the G-band (I_D/I_G). As shown in Figure 2(f), the I_D/I_G ratio for all prepared samples was approximately 1.1, indicating a similar degree of structural defects and demonstrating consistency in defect distribution across the carbon supports of the four electrocatalysts [24].

XPS was further employed to investigate the surface elemental composition and chemical states of the four synthesized electrocatalysts. The elemental spectra obtained after peak deconvolution of the XPS results are shown in Figure 3. Figure 3(a) displays the Pt 4f spectra of the four as-prepared

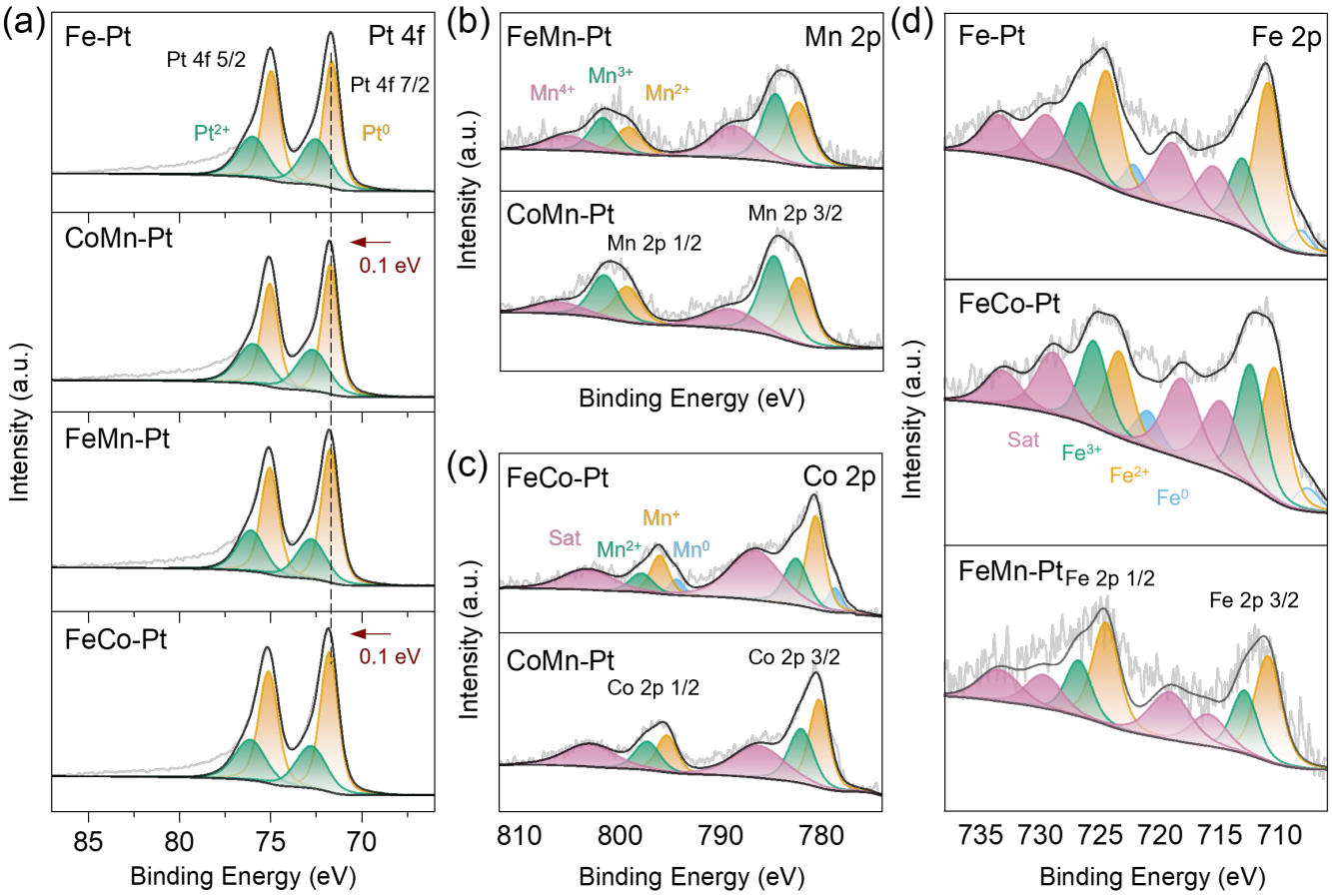


Figure 3: XPS spectra of the (a) Pt 4f, (b) Mn 2p, (c) Co 2p, and (d) Fe 2p core level peaks of the Pt catalysts.

electrocatalysts; the Pt 4f 5/2 and Pt 4f 7/2 signals can be resolved into two spin-orbit doublets [25], where the primary doublet at 71.6 eV and 74.9 eV is attributed to metallic Pt^0, while the minor doublet at 72.5 eV and 76 eV corresponds to Pt^{2+}. This indicates that Pt^0 is the dominant species on the electrocatalyst surface, accompanied by a small amount of Pt^{2+} resulting from surface oxidation. Notably, compared to the Pt 4f 5/2 and Pt 4f 7/2 binding energies of Pt^0 in Fe-Pt, the binding energies of Pt^0 in CoMn-Pt, FeMn-Pt, and FeCo-Pt exhibit positive shifts of 0.1 eV, 0.1 eV, and 0.2 eV, respectively. These results demonstrate that different transition metal combinations exert varying effects on the electronic structure of platinum [26], with the FeCo combination exerting the most significant influence by conducting a mechanism similar to "dual-metal electron pump" [27]. Figure 3(b) shows the Mn 2p spectra for the CoMn-Pt and FeMn-Pt electrocatalysts, which can be deconvoluted into Mn^{2+}, Mn^{3+} and Mn^{4+} components [28]. Figure 3(c) presents the Co 2p spectra for CoMn-Pt and FeCo-Pt, resolvable into Co^{2+}, Co^{3+} species and satellite structure. In contrast, the FeCo-Pt sample exhibits an additional set of peaks corresponding to metallic Co^0 alongside the aforementioned peaks; this observation aligns with the TEM and XRD analysis results, further confirming the formation of an FeCo alloy within the system [29]. Figure 3(d) shows the Fe 2p spectrum of the electrocatalyst; four peaks were identified through fitting, corresponding to the satellite peak, Fe^{3+}, Fe^{2+}, Fe^0 and satellite structure [29], respectively. Notably, the characteristic peak of Fe^0 in the FeCo sample confirms the formation of the FeCo alloy, validating the results obtained from XRD and TEM analyses.

3 Electrochemical Measurement and Component Performance

The rotating disk electrode (RDE) is a common electrochemical technique used to evaluate the catalytic performance of electrocatalysts; its advantage lies in providing stable and reproducible measurements under strictly controlled experimental conditions. To systematically investigate the catalytic activity of the catalysts toward HOR, this study employed a conventional three-electrode system, utilizing an RDE coupled with an electrochemical workstation, to conduct electrochemical tests on four synthesized electrocatalysts. Figure 4(a) presents the linear sweep voltammetry (LSV) results for FeCo-Pt in 0.1 M $HClO_4$ electrolyte saturated with N_2 and H_2, respectively. At potentials exceeding 0.1 V vs. RHE, the current density under N_2-saturated conditions was negligible, indicating the absence of redox-active species in the solution; in contrast, the current density increased significantly in the H_2-saturated electrolyte, demonstrating the catalyst's ability to effectively catalyze the electrochemical oxidation of H_2 in the 0.1 M $HClO_4$ medium. The LSV curves for the FeCo-Pt, FeMn-Pt, CoMn-Pt, and Fe-Pt in H_2-saturated electrolyte were obtained as shown in Figure 4(b). Both FeCo-Pt and FeMn-Pt exhibited a current density of 2.92 mA/cm^2 at 0.1 V vs. RHE, notably higher than those of Fe-Pt (2.72 mA/cm^2) and CoMn-Pt (2.62 mA/cm^2). These

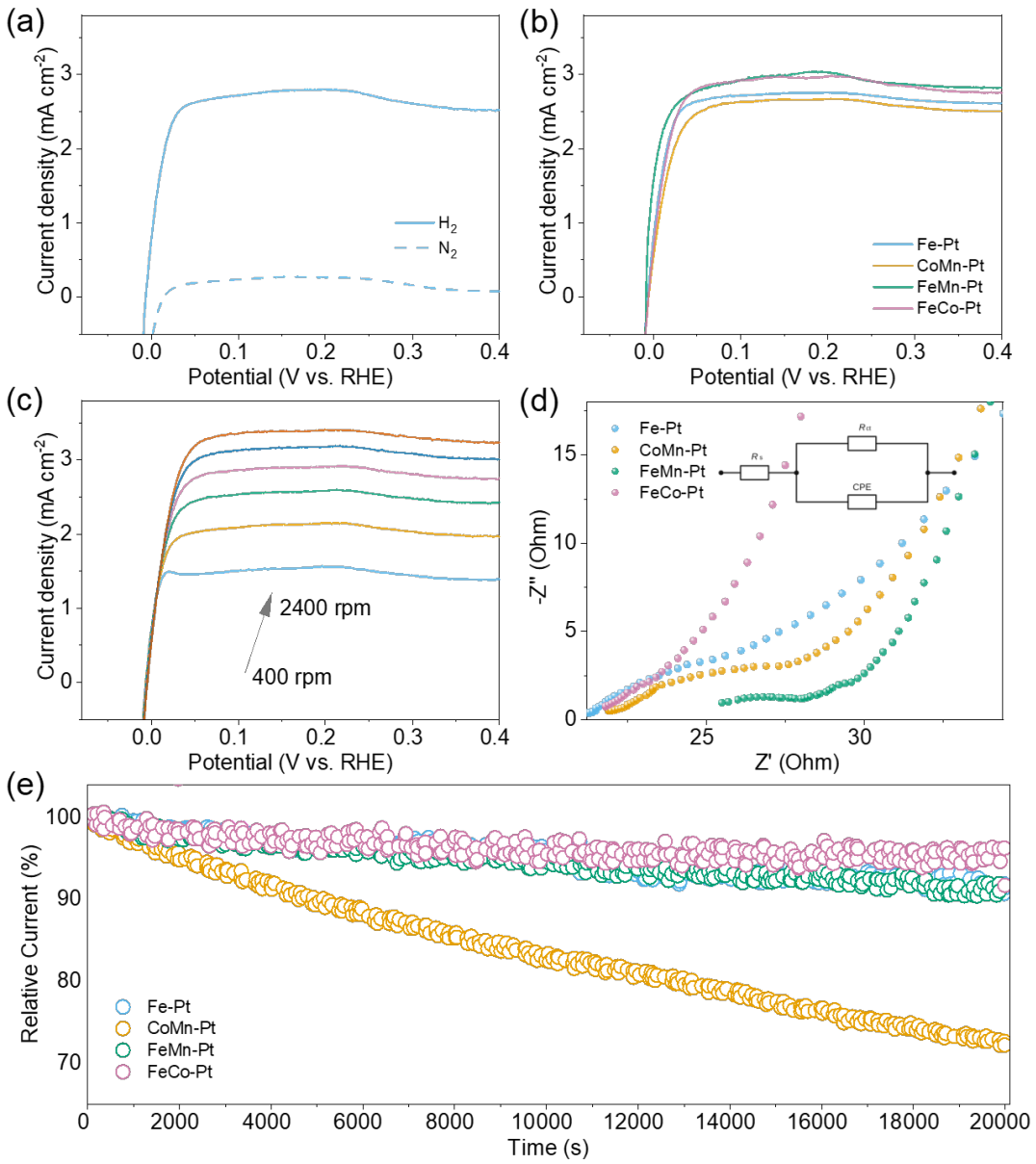


Figure 4: (a)LSV curves for HOR in H_2 and N_2, (b) HOR curves for HOR in H_2 of the synthesized four Pt electrocatalysts. LSV (c) and Nyquist (d) plots of FeCo-Pt at multiple rotation rates (the rotation speed interval was 400 rpm). (e) Durability test of the four Pt electrocatalysts.

results indicate that FeCo-Pt and FeMn-Pt possess superior HOR catalytic activity, which could be attributed to the synergistic effects between Fe and Co (or Fe and Mn) in modulating the electronic structure of Pt by acting as nearby electronic pump, thereby enhancing the catalyst's activity and electrochemical reaction kinetics. Figure 4(c) shows the polarization curves of FeCo-Pt at various rotation speeds in H_2-saturated 0.1 M $HClO_4$ electrolyte; the limiting current density increases with the rotation speed of the RDE, consistent with the classical mass-transport-controlled mechanism. Fitting the data yields a slope of 13.61 mA^{-1} cm^2 $rpm^{1/2}$ at 30 mV for the kinetic polarization curve of FeCo-Pt-C, which is very close to the theoretical value of 15.06 mA^{-1} cm^2 $rpm^{1/2}$ indicating that the HOR on the FeCo-Pt catalyst proceeds via a two-electron transfer process [30]. EIS was also conducted as shown in Figure 4(d). The Nyquist plots for all catalysts consist of a capacitive arc in the high-to-medium frequency region and a mass-transfer tail in the low-frequency region. Notably, the FeCo-Pt catalyst exhibits the smallest capacitive arc diameter in the high-to-medium frequency region, indicating the lowest charge-transfer resistance (R_{ct}) and confirming its superior intrinsic kinetic activity for the HOR [31]. This indicates that the synergistic modulation by the transition metals Fe and Co exerts a more pronounced positive effect on the catalyst's electronic structure and interfacial properties, effectively reducing the kinetic resistance to charge transfer and thereby accelerating the HOR.

Catalyst durability is a key indicator for assessing potential industrial application. To evaluate the durability of four electrocatalysts, chronoamperometric (*i*–*t*) tests were conducted using the RDE. Changes in current density over time were continuously monitored, and the resulting stability curves are shown in Figure 4(e). After 20000 s of operation under the specified conditions (0.1 V), the current density

of the FeCo-Pt catalyst decreased by only 4.41%, whereas those of the FeMn-Pt, CoMn-Pt, and Fe-Pt catalysts declined by 8.28%, 27.63%, and 8.50%, respectively. These results demonstrate the exceptional stability of FeCo-Pt under acidic HOR conditions, further confirming that the formation of a FeCo alloy structure enhances durability and providing strong support for its practical application.

As a critical component of electrochemical hydrogen sensors, the anode's HOR performance is vital to the sensor's response to hydrogen. The catalyst's HOR activity, stability, and poison tolerance must ultimately be validated in a device environment that closely simulates actual conditions. To this end, the prepared catalyst was fabricated into a membrane electrode assembly (MEA) based on previously reported procedures and systematically evaluates their hydrogen response behavior under conditions closely resembling real-world sensors, thereby providing device-level insights for the development of high-performance hydrogen sensors [32]. Hydrogen sensing MEAs were fabricated via the hot-press transfer method [33, 34] using commercially available 20% Pt/C as the cathode catalyst and FeCo-Pt, FeMn-Pt, and Fe-Pt as anode catalysts (all with a Pt loading of $0.1 + 0.1$ mg/cm^2 and N212 membrane with a thickness of $\sim$50 μm was selected as electrolyte). During device performance testing, H_2 and an NH_3/H_2 mixture were sequentially fed to the anode, while no gas was supplied to the cathode; this setup aimed to evaluate the performance of the various anode catalysts in an ammonia-containing environment and to elucidate the extent to which synergistic elemental modulation influences ammonia tolerance.

The configuration of the electrochemical hydrogen sensor based on a high-efficiency HOR anode used in this study is shown in Figure 5(a). The core assembly features a circular, three-in-one structure, and hydrogen detection is achieved by connecting the anode and cathode to a circuit and applying specific current or voltage conditions. By clamping the sensing component onto the test fixture, the component's response capability for hydrogen detection under actual operating conditions, including in the presence of ammonia interference, can be effectively evaluated. As shown in Figure 5(b), at current densities of 0.5 A/cm^2 and 1.0 A/cm^2, the voltages required for the FeCo-Pt catalyst are 9.8 mV and 27.9 mV lower than those for the FeMn-Pt catalyst, and 14.8 mV and 38.0 mV lower than those for the Fe-Pt catalyst, respectively; this indicates that FeCo-Pt possesses superior electrocatalytic activity towards hydrogen sensing compared to FeMn-Pt and Fe-Pt, enabling higher current densities at the same control voltage. Testing conducted after introducing 5000 ppm NH_3/H_2 at the anode (Figure 5(c)) reveals that at a current density of 0.5 A/cm^2, the voltage required for the FeCo-Pt catalyst is 260.2 mV and 322.9 mV lower than that for the FeMn-Pt and Fe-Pt catalysts, respectively. This result demonstrates the superior resistance of FeCo-Pt to ammonia poisoning by exhibiting a higher response current to hydrogen in an ammonia-containing environment. Overall, in pure H_2, the required applied voltage increases gradually and almost linearly with increasing output current, while remaining consistently low. In contrast, with the NH_3/H_2 mixture, the initial applied voltage is significantly higher and rises sharply as the output current increases, highlighting the severe poisoning effect of ammonia on the electrocatalysts. As shown in Figures 5(d),(e), at a current density of 0.5 A/cm^2, the performance of FeCo-Pt in the absence and presence of NH_3 mixture surpasses that of FeMn-Pt by 18.3% and 40.6%, and that of Fe-Pt by 24.9% and 50.4%, respectively; these results indicate that FeCo-Pt not only exhibits exceptional HOR activity but also demonstrates excellent ammonia tolerance. In contrast, the performance of comparison FeMn-Pt and Fe-Pt samples catalysts declined more significantly under identical conditions. Stability is a fundamental prerequisite for electrochemical hydrogen sensors to achieve long-term online monitoring. Therefore, as shown in Figure 5(f), a continuous operational durability testing lasting 3600 s was conducted on an MEA utilizing FeCo-Pt under conditions of a 5000 ppm NH_3/H_2 gas mixture and a current density of 0.5 A/cm^2. After operation, the FeCo-Pt catalyst retained 86.6% of its initial electrocatalytic efficiency. These results demonstrate that FeCo-Pt not only exhibits excellent HOR performance but also maintains high stability under ammonia-poisoning conditions, since hydrogen sensors are typically in a standby state. Its stability performance should be sufficient to support sensors developed subsequently in serving real-world scenarios for several years or more. This indicates that alloying with Fe and Co significantly alters the catalyst's electronic structure and enhances its ammonia tolerance through the hypothesized "dual-metal electron pump" effect, further proving that the synergistic modulation of platinum's electronic structure by multiple transition elements is an effective strategy for significantly improving the hydrogen-sensing catalyst's resistance to ammonia poisoning.

4 Conclusions

To address the design requirements for anodes in hydrogen electrochemical sensors with high resistance to ammonia interference, this study proposes a "bimetallic electron pump" strategy to modulate conventional Pt catalysts. By employing controlled heat treatment to form transition metal alloys, the electronic structure of Pt is precisely and directionally tuned. Compared to doping with a single transition metal, the preferred FeCo alloy acts as a powerful bimetallic electron pump, directionally supplying sufficient electrons to the neighboring Pt. Under an NH_3/H_2 atmosphere, the sensing HOR performance of the FeCo-Pt anode surpasses that of FeMn-Pt and Fe-Pt by 40.6% and 50.4%, respectively; furthermore, it maintains a robust, continuous response for hydrogen detection even in the presence of high ammonia concentrations (5000 ppm). This advantage stems from the FeCo alloy's precise modulation of the Pt electronic structure, which reduces Pt's adsorption affinity for NH_3 while preserving the high activity required for the HOR. This strategy leveraging a bimetallic electron pump to synergistically tune the electronic structure of Pt offers a novel approach to designing anode catalysts for ammonia-tolerant hydrogen electrochemical sensors and provides valuable insights for catalyst design in fields such as proton exchange membrane fuel cell anodes and direct ammonia fuel cell anodes.

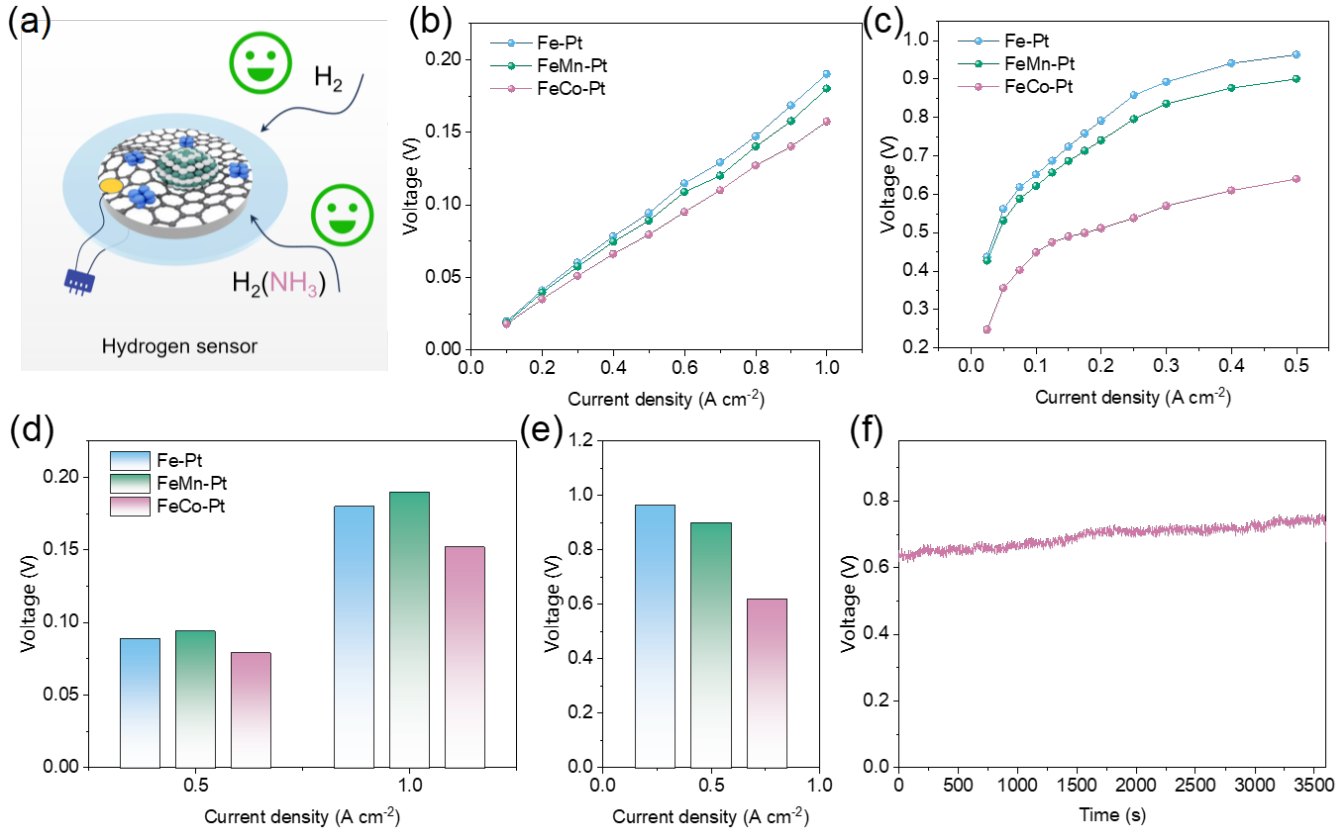


Figure 5: (a) Schematic diagram of the structure of an ammonia-interference-resistant electrochemical hydrogen sensor assembly. I-V curves at pure H2 (b) and 5000 ppm NH3/H2 (c) for Fe-Pt, FeMn-Pt, and FeCo-Pt. Driving voltage at specific current density of Fe-Pt, FeMn-Pt, and FeCo-Pt at H2 (d) and 5000 ppm NH3/H2 (e) condition. (f) Continuous operational durability testing of the sensor assembly with FeCo-Pt catalyst as anode under 5000 ppm NH3/H2.

Fundings

This work was financially supported by the National Key Research and Development Program of China (No. 2023YFB4005604).

Author Contributions

Conceptualization, R.W.; methodology, C.J. and R.W.; investigation, C.J., A.Z., Y.Z. and Z.H.; writing—original draft, C.J.; writing—review and editing, R.W. and H.T.; supervision, R.W. and H.T. All authors have read and agreed to the published version of the manuscript.

Conflict of Interest

The authors declare no conflicts of interest.

References

[1] Angelico, R., Giametta, F., Bianchi, B., Catalano, P.: Green Hydrogen for Energy Transition: A Critical Perspective. Energies **18**(2), 404 (2025). https://doi.org/10.3390/en18020404

[2] Yao, Y., Tan, L., Chen F., Pan A., Ma Q., Zhao J., Kang R.: Hydrogen energy industry in China: The current status, safety problems, and pathways for future safe and healthy development. Safety Science **186**, 106808 (2025). https://doi.org/10.1016/j.ssci.2025.106808

[3] Wang, S., Pan, J., He, H., Qiu, J., Chai, M., Bi, J., Wang, Z., Hao, X., Zhang, R., Li, C.: Overview on the Current Global Market and Sustainability of Hydrogen Supply Chain Based on China. Clean Energy and Sustainability **4**(2), 10011 (2026). https://doi.org/10.70322/ces.2026.10011

[4] Kumar, L., Sleiti, A.K.: A comprehensive review of hydrogen safety through a metadata analysis framework. Renewable & Sustainable Energy Reviews **214**, 115509 (2025). https://doi.org/10.1016/j.rser.2025.115509

[5] Yang, F., Wang, T., Deng, X., Dang, J., Huang, Z., Hu, S., Li, Y., Ouyang, M.: Review on hydrogen safety issues: Incident statistics, hydrogen diffusion, and detonation process. International Journal of Hydrogen Energy **46**(61), 31467–31488 (2021). https://doi.org/10.1016/j.ijhydene.2021.07.005

[6] Liu, X., Chen, X., Ju, J., Wang X., Mei Z., Qu, H., Xu, Y., Zeng, X.: Platinum-Nickel Bimetallic Nanosphere-Ionic Liquid Interface for Electrochemical Oxygen and Hydrogen Sensing. ACS Applied Nano Materials **2**(5), 2958–2968 (2019). https://doi.org/10.1021/acsanm.9b00380

[7] Lü, Y., Ling, Y., Ma, J., Ren, F., Xu, J.: Pd Doped TiO2 Nanotube Arrays: Preparation and Hydrogen-Sensing Performance (In Chinese). Chinese Journal of Inorganic Chemistry **26**, 627–632 (2010).

[8] Seleka, W.M., Ramohlola, K.E., Modibane, K.D., Makhado E.: Conductive chitosan/polyaniline hydrogel: A gas sensor for room-temperature electrochemical hydrogen sensing. International Journal of Hydrogen Energy **68**, 940–954 (2024). https://doi.org/10.1016/j.ijhydene.2024.04.240

[9] Siga, M.D.W., Sonda, K., Putri, G.K., Tsugawa, T., Yamaguchi, M., Kiyozawa, T., Ahmad, M.S., Inomata, Y., Hatakeyama, K., Ida S., *et al.*: Low-Power Electrochemical Hydrogen Gas Sensor Using Pd-Decorated Graphene Oxide Electrode. Journal of Physical Chemistry C **130**(20), 7117–7126 (2026). https://doi.org/10.1021/acs.jpcc.6c00622

[10] Jin, C., Wu, F., Tang, H., Pan, H., Chen Z., Wang, R., Meng, Z., Li, J., Tang, H.: Confined tuning of the charge distribution of Pt electrocatalyst for reinforcing anti-poisoning ability: Toward efficient separation of hydrogen from gases containing ammonia. Chemical Engineering Journal **475**, 146139 (2023). https://doi.org/10.1016/j.cej.2023.146139

[11] Peng, L., Tian, H., Cui, X., Su, L., Meng, G., Ma, Z., Cao, S., Shi, J.: Dual synergetic catalytic effects boost hydrogen electric oxidation performance of Pd/W18O49. Nano Research **14**, 2441–2450 (2021). https://doi.org/10.1007/s12274-020-3248-0

[12] Yang, X., Li, S., Guo, J., Meng, Z., Wang, Y.: Ammonia Poisoning Behaviors on Pt/C Catalyst Layer in PEMFC. Journal of the Electrochemical Society **173**, 186502 (2026). https://doi.org/10.1149/1945-7111/aea714

[13] Aziz, M., Wijayanta, A.T., Nandiyanto, A.B.D.: Ammonia as Effective Hydrogen Storage: A Review on Production, Storage and Utilization. Energies **13**(12), 3062 (2020). https://doi.org/10.3390/en13123062

[14] Zhu, C., Guan, B., Zhuang, Z., Chen, J., Ma, Z., Hu, X., Zhao, S., Shu, K., Dang, H., Gao, J., *et al.*: Research status and advances of ammonia and hydrogen in the field of energy: Combined utilization. Energy Conversion and Management **327**, 119610 (2025). https://doi.org/10.1016/j.enconman.2025.119610

[15] Verdaguer-Casadevall, A., Hernandez-Fernandez, P., Stephens, I.E.L., Chorkendorff, I., Dahl, S.: The effect of ammonia upon the electrocatalysis of hydrogen oxidation and oxygen reduction on polycrystalline platinum. Journal of Power Sources **220**, 205–210 (2012). https://doi.org/10.1016/j.jpowsour.2012.07.141

[16] Zhao, Y., Wang, X., Wang, R., Wu, F., Duan, W., Li, H., Tang, H.: Ammonia-resistant Pt-based HOR catalyst with Fe/Y co-regulation for high-efficiency hydrogen purification enabled by machine learning. Science China-Materials **68**, 2397–2407 (2025). https://doi.org/10.1007/s40843-025-3399-3

[17] Wang, Y., Gao, F., Zhang, X., Yang, Y., Liao, J., Niu, Z., Qin, S., Yang, P., Yu, P., Sun, M., *et al.*: Efficient NH_3-Tolerant Nickel-Based Hydrogen Oxidation Catalyst for Anion Exchange Membrane Fuel Cells. Journal of the American Chemical Society **145**(31), 17485–17494 (2023). https://doi.org/10.1021/jacs.3c06903

[18] Li, L., Shen, Q., Cheng, J., Hao, Z.: Catalytic oxidation of NO over TiO_2 supported platinum clusters I. Preparation, characterization and catalytic properties. Applied Catalysis B-Environmental **93**(3-4), 259–266 (2010). https://doi.org/10.1016/j.apcatb.2009.09.037

[19] Oliveira, A.S., Cueto, J., Alonso-Doncel, M.M., Kubu, M., Cejka, J., Serrano, D.P., García-Muñoz, R.A.: Propane dehydrogenation over Pt and Ga-containing MFI zeolites with modified acidity and textural properties. Catalysis Today **427**, 114437 (2024). https://doi.org/10.1016/j.cattod.2023.114437

[20] Liu, P., Sun, Y., Luo, J., Dong, Z., Zhang, P., Zhong, S., Wei, Y., Song, W., Wang, Y., Li, Z., *et al.*: CoFe alloy embedded in ultra-thin nitrogen-doped carbon nanosheets derived from CoFe LDH as efficient oxygen reduction electrocatalyst for Zn-air batteries. Nano Research **18**(2), 94907139 (2025). https://doi.org/10.26599/nr.2025.94907139

[21] Chen, Y., Meng, Z., Wei, X., Wu, M., Xiong, Y., Tang, H., Wang, R., Tian, T., Wang, D., Tang, H.: Tellurium-Nitrogen-Carbon Support Boosting Platinum Catalysis in High-Efficiency Proton Exchange Membrane Fuel Cells. Angewandte Chemie-International Edition **64**, e202512315 (2025). https://doi.org/10.1002/anie.202512315

[22] Miao, P., Yu, Z., Chen, W., Zhou, R., Zhao, W., Chen, K., Kong, J.: Synergetic Dielectric and Magnetic Losses of a Core-Shell Co/MnO/C Nanocomplex toward Highly Efficient Microwave Absorption. Inorganic Chemistry **61**(3), 1787–1796 (2022). https://doi.org/10.1021/acs.inorgchem.1c03749

[23] Jin, C., Liao, Y., Zhang, A., Zhao, S., Wang, R., Li, J., Tang, H.: Low-Pt anodes with gradient molybdenum isomorphism for high performance and anti-CO poisoning PEMFCs. Nano Energy **122**, 109305 (2024). https://doi.org/10.1016/j.nanoen.2024.109305

[24] Yang, C., Sun, F., Zhang, Y., Qu, Z., Zuo, J., Zhou, W., Gao, J., Liu, S., Lu, Y.: Unveiling the coupling effect of sp^2 domain size and local active sites in switching the selectivity of nanocarbon catalysts toward the oxygen electro-reduction. Nature Communications **16**, 11270

(2025). https://doi.org/10.1038/s41467-025-66161-5

[25] Jin, K., Lu, X., Li, Z., Zhao, G., Li, W., Zhang, X., Wang, H., Wu, J., Xie, X., Zhao, L., *et al.*: Catalytic Aqueous Phase Conversion of Cellulose to Ethanol over Multifunctional $Pt/WO_X/SiO_2$ Catalysts. Energy & Fuels **39**(15), 7339–7348 (2025). https://doi.org/10.1021/acs.energyfuels.5c00206

[26] Xu, Q., Wang, Z., Shi, J., Su, Y., Feng, X., Ji, W., Au, C.-T.: Ultra-Fine Pt Entities on High-Index CeO2(112) Facet Significantly Boosting Low Temperature Water-Gas Shift Reaction. ACS Catalysis **16**(1), 680–693 (2026). https://doi.org/10.1021/acscatal.5c07417

[27] Alghannam, A., Pattison, A.J., Das, S., Dun, C., Ercius, P., Urban, J.J., Gates, B.C., Bell, A.T.: Unraveling the Unique Behavior of Atomically Dispersed Pt on Zeolite Fe-DeAlBEA for Catalyzing Propane Dehydrogenation with Cofed Hydrogen. Journal of the American Chemical Society **147**(16), 13784–13798 (2025). https://doi.org/10.1021/jacs.5c01730

[28] Guo, S., Chen, H., Wang, W., Sun, X., Zhang, J., Yi, Z., Feng, W., Liu, G.: Synergistic effect of built-in electric field and mixed-valence Mn2+/Mn3+/Mn4+ species in MnS/BiOCl heterostructure promotes photocatalytic H2 production. Journal of Environmental Chemical Engineering **14**(6), 124848 (2026). https://doi.org/10.1016/j.jece.2026.124848

[29] Wang, X., Xu, X., Nie, Y., Wang, R., Zou, J.: Electronic-State Modulation of Metallic Co-Assisted Co7Fe3 Alloy Heterostructure for Highly Efficient and Stable Overall Water Splitting. Advanced Science **10**, 2301961 (2023). https://doi.org/10.1002/advs.202301961

[30] Liu, Y., Cheng, L., Zhou, S., Yang, Y., Niu, C., Isimjan, T.T., Wang, B., Yang, X.: Revealing interfacial charge redistribution of homologous Ru-RuS2 heterostructure toward robust hydrogen oxidation reaction. Journal of Energy Chemistry **94**, 332–339 (2024). https://doi.org/10.1016/j.jechem.2024.03.007

[31] Derkaoui, K., Bencherifa, I., Elfiad, A., Boukhouidem, K., Kechouane, M., Mebdoua, Y., Hadjersi, T.: Nickel aluminate spinel as a noble-metal-free electrocatalyst for alkaline hydrogen evolution reaction. Reaction Kinetics, Mechanisms and Catalysis **139**, 2349–2369 (2026). https://doi.org/10.1007/s11144-026-03080-6

[32] Li, W., Huang, L., Sun, H., Wang, B., Lu, Q., Liang, X., Liu, F., Liu, F., Sun, P., Lu, G.: Room temperature hydrogen sensor based on Nafion and Pd/CF sensing electrode. Sensors and Actuators B: Chemical **366**, 132014 (2022). https://doi.org/10.1016/j.snb.2022.132014

[33] Tang, H., Wang, S., Jiang, S., Pan, M.: A comparative study of CCM and hot-pressed MEAs for PEM fuel cells. Journal of Power Sources **170**(1), 140–144 (2007). https://doi.org/10.1016/j.jpowsour.2007.03.062

[34] Hong, Y., Liu, C., Cao, X., Chen, Y., Chen, C., Chen, Y., Pan, Z.: Process Evaluation of the Metal-Organic Frameworks for the Application of Personal Protective Equipment with Filtration Function. Polymers **10**(12), 1386 (2018). https://doi.org/10.3390/polym10121386